Retrodifferentiation of human tumor hepatocytes to stem cells leads to metabolic reprogramming and chemoresistance

Karim Fekir, Hélène Dubois-Pot-Schneider, Romain Desert, Yoann Daniel, Denise Glaise, Claudine Rauch, Fabrice Morel, Bernard Fromenty, Orlando Musso, Florian Cabillic, et al.

▶ **To cite this version:**

Karim Fekir, Hélène Dubois-Pot-Schneider, Romain Desert, Yoann Daniel, Denise Glaise, et al.. Retrodifferentiation of human tumor hepatocytes to stem cells leads to metabolic reprogramming and chemoresistance. Cancer Research, 2019, 79 (8), pp.1869-1883. 10.1158/0008-5472.CAN-18-2110 . hal-02087900

HAL Id: hal-02087900

https://univ-rennes.hal.science/hal-02087900

Submitted on 6 Jun 2019

HAL is a multi-disciplinary open access archive for the deposit and dissemination of scientific research documents, whether they are published or not. The documents may come from teaching and research institutions in France or abroad, or from public or private research centers.

L'archive ouverte pluridisciplinaire **HAL**, est destinée au dépôt et à la diffusion de documents scientifiques de niveau recherche, publiés ou non, émanant des établissements d'enseignement et de recherche français ou étrangers, des laboratoires publics ou privés.

Retrodifferentiation of human tumor hepatocytes to stem cells leads to metabolic reprogramming and chemoresistance

Karim Fekir[1], Hélène Dubois-Pot-Schneider[1], Romain Désert[1], Yoann Daniel[1], Denise Glaise[1], Claudine Rauch[1], Fabrice Morel[1], Bernard Fromenty[1], Orlando Musso[1], Florian Cabillic[1,2], and Anne Corlu[1#.]

[1] INSERM, Univ Rennes, INRA, Institut NuMeCan (Nutrition, Metabolisms and Cancer) F-35000 Rennes, France

[2] CHU Rennes, Laboratoire de Cytogénétique et Biologie Cellulaire, F-35000 Rennes, France

Running title: Reversing chemoresistance in HCC stem cells

Abbreviations list

ANGPTL4, angiopoietin-like 4; CSCs, cancer stem cells; DCA, dichloroacetate; GSEA, gene set enrichment analysis; HCC, hepatocellular carcinoma; IPA, ingenuity pathway analysis; ITGB, integrin; MMP, metalloproteinase; PDK4, pyruvate dehydrogenase kinase 4; PDH, pyruvate deshydrogenase; PPARG, peroxisome proliferator-activated receptor γ; PPARGC1A, PPARG coactivator 1α; OXPHOS, oxidative phosphorylation; SP, side population; NSP, non-side population; TCA, tricarboxylic acid cycle; TMA, tissue microarray.

Corresponding author contact information

Anne Corlu PhD

Institute Nutrition, Metabolisms and Cancer (NuMeCan)

Accepted manuscript

Hôpital Pontchaillou, Rue Henri le Guilloux, 35033 Rennes, France

E-mail: anne.corlu@inserm.fr; Phone: +33 (0)2 23 23 38 70; Fax: +33 (0)2 99 54 01 37

Conflicts of interest: The authors declare no potential conflicts of interest

Accepted manuscript

.

SIGNIFICANCE STATEMENT

Restoring mitochondrial function in human hepatocellular carcinomas overcomes cancer resistance

Accepted manuscript

ABSTRACT

Human hepatocellular carcinoma (HCC) heterogeneity promotes recurrence and therapeutic resistance. We recently demonstrated that inflammation favors hepatocyte retrodifferentiation into progenitor cells. Here we identify the molecular effectors that induce metabolic reprogramming, chemoresistance, and invasiveness of retrodifferentiated HCC stem cells. Spheroid cultures of human HepaRG progenitors (HepaRG-Spheres), HBG-BC2, HepG2, and HuH7 cells and isolation of side population (SP) from HepaRG cells (HepaRG-SP) were analyzed by transcriptomics, signaling pathway analysis, and evaluation of chemotherapies. Gene expression profiling of HepaRG-SP and HepaRG-Spheres revealed enriched signatures related to cancer stem cells, metastasis, and recurrence and showed that HepaRG progenitors could retrodifferentiate into an immature state. The transcriptome from these stem cells matched that of proliferative bad outcome HCCs in a cohort of 457 patients. These HCC stem cells expressed high levels of cytokines triggering retrodifferentiation and displayed high migration and invasion potential. They also showed changes in mitochondrial activity with reduced membrane potential, low ATP production, and high lactate production. These changes were in part related to angiopoietin-like 4 (ANGPTL4)-induced upregulation of pyruvate dehydrogenase kinase 4 (PDK4), an inhibitor of mitochondrial pyruvate dehydrogenase. Upregulation of ANGPTL4 and PDK4 paralleled that of stem cells markers in human HCC specimens. Moreover, the PDK4 inhibitor dichloroacetate reversed chemoresistance to sorafenib or cisplatin in HCC stem cells derived from four HCC cell lines. In conclusion, retrodifferentiated cancer cells develop enhanced invasion and therapeutic resistance through ANGPTL4 and PDK4. Therefore, restoration of mitochondrial activity in combination with chemotherapy represents an attractive therapeutic approach in HCC.

Accepted manuscript

INTRODUCTION

Hepatocellular carcinoma (HCC) is the third most common cause of cancer-related deaths worldwide. Despite recent progress in treatment, tumor recurrence remains high. HCCs show heterogeneous cell populations, suggesting that liver tumors may originate from different cell types(1). Although mature hepatocytes have long been considered as the target of oncogenic transformation, it is now proposed that HCCs may arise from different cells of the hepatic lineage i.e., hepatocytes, hepatoblasts and hepatic progenitors(2,3). Furthermore, the presence of cancer stem cells (CSCs) in HCCs derived from these cell types suggest that any cell of the hepatic lineage could acquire stem cell properties. *In vitro* experiments have demonstrated that the inflammatory microenvironment promotes the retrodifferentiation of tumor-derived hepatocytes toward bipotent progenitor cells(4) and human and mouse hepatocytes can undergo reversible ductal metaplasia in response to injury *in vivo*(5). These new insights on the plasticity of differentiated tumor cells add to the complexity of the origin of CSCs and reinforce the hypothesis of their contribution to the cellular heterogeneity and chemoresistance in HCC(6). In addition, CSCs are spared by cancer chemotherapy that usually affects differentiated and dividing cells to reduce the tumor mass.

CSCs share properties with normal adult stem cells. They are able to self-renew by symmetric division but can also undergo asymmetric division, which preserves the stem cell pool, and give rise to a progeny of transit-amplifying cells that commit to a lineage differentiation program. CSCs are thought to give rise to all cell types within the tumor and can promote malignant progression. They exhibit drug resistance by having a low proliferation rate and high expression of xenobiotic transporters(7). Similar dysregulations of signaling pathways for stemness, proliferation and differentiation in normal stem cells have been identified in CSCs and can contribute to tumor formation(8). Recent data unveiled unexpected metabolic heterogeneity within the tumor mass(9) and suggested that CSC could harbor distinct

Accepted manuscript

metabolic phenotypes from differentiated tumor cells in various tissues. However, the metabolic profile of CSCs is controversial. Metabolic plasticity could allow CSCs to alternatively rely on either glycolysis or oxidative phosphorylation (OXPHOS) rather than acquiring a stereotypical energy metabolism profile(10). Therefore, a better understanding of the functional properties of retrodifferentiated cells is crucial for developing new therapeutic approaches that aim to eradicate both CSCs and differentiated cancer cells.

Among HCC cell lines, some retain a poorly differentiated phenotype such as HuH7 and HepG2 cells whereas others display reversible differentiation program e.g. HBG-BC2 (BC2) and HepaRG cell lines(11,12). HepaRG cells differ from BC2 cells in that they display a higher potential for plasticity, which ranges from liver progenitors to highly differentiated hepatocyte- and biliary-like cells. Furthermore, differentiated HepaRG cells are able to retrodifferentiate into progenitor cells when seeded at low density(12). Recently, we have demonstrated that inflammatory cytokines and transforming growth factor β (TGFβ) promote the retrodifferentiation of mature HepaRG hepatocyte-like cells and that retrodifferentiated progenitors express a genetic program typical of HCCs with aggressive behavior and unfavorable outcome(4). Here, we show that differentiated HepaRG hepatocyte-like cells not only retrodifferentiate to HCC progenitor cells, but also can acquire stem cell features under particular conditions. The HepaRG-derived stem cells expressed a transcriptomic program that was similar to proliferative, bad outcome HCCs in two separate cohorts totaling 457 patients. Emergence of the CSC phenotype is associated with a modulation of invasion, inflammation, redox homeostasis and energy metabolism, initiated in part by angiopoietin like-4 (ANGPTL4) and mitochondrial pyruvate dehydrogenase kinase (PDK) 4. We demonstrate that the upregulation of PDK4 was associated to chemoresistance that could be successfully reversed by the PDK4 inhibitor dichloroacetate (DCA), in four HCC cell lines.

Accepted manuscript

Therefore, targeting stem cells by restoring mitochondrial pyruvate oxidation in combination with chemotherapy appears as a promising approach to treat HCC.

Accepted manuscript

MATERIALS AND METHODS

Sphere culture

HepaRG and BC2 cells were originally isolated in the laboratory(11,12) and grown in William's E medium containing 0.025g/L pyruvic acid and supplemented with 10% fetal calf serum (FCS), 5μg/mL insulin and hydrocortisone hemisuccinate (5.10^{-5} and 7.10^{-7}M, respectively). HepG2 and HuH7 cells, obtained from American Tissue culture collection and European Collection of Authenticated Cell Cultures, were grown in Eagle's minimum essential medium (MEM) and Dubelco's modified MEM, (DMEM) respectively, both supplemented with 10% FCS. For the sphere culture, cells were seeded in the same media with 2% FCS and 50-fold reduced concentration of insulin and hydrocortisone hemisuccinate, for 5 days. Then, cells were detached and seeded in ultra-low attachment plates in DMEM/F12 medium supplemented with 20% knockout serum replacement, 1mM L-glutamine, 1% nonessential amino acids, 0.1mM β-mercaptoethanol, and 4ng/mL fibroblast growth factor 2 (FGF2, MiltenyiBiotec) for 5 more days. Medium was renewed at day 1 and 3. The use of human Embryonic Stem (hES) cells H9 (WA09 obtained from WiCell) was approved by the French Biomedicine Agency (No.RE10-013 I/C/R). Cell line authentication was performed with AuthentiFiler™ PCR Amplification Kit - Genotype Comparison Tool v1.0 (Life Technologies) and mycoplasma testing was performed twice a year with MycoAlert Mycoplasma detection kit (Lonza).

Side population quantification and sorting by flow cytometry

At day 4, HepaRG, HuH7 and HepG2 cells were suspended at 1 x 10^6 cells/mL in Hank's balanced salt solution supplemented with 3% FCS and 10mM HEPES, and incubated for 90 minutes with 20μg/mL Hoechst 33342 (Sigma-Aldrich), with or without the P-glycoprotein inhibitor verapamil (50μM, Sigma-Aldrich). Then, 1μg/mL propidium iodide (Pharmingen)

Accepted manuscript

was added and cells were filtered through a 40µm strainer to obtain a single cell suspension. Cell analysis and sorting were performed using Becton Dickinson FACSAria III™. Fluorescence emission of Hoechst 33342 was measured through 450DF20 BP (Hoechst blue) and 675DF20 BP (Hoechst red) optical filters. Dead cells were discriminated using propidium iodide labeling. Cells able to efflux Hoescht 33342 are referred to as side population (SP) cells.

Microarray analysis and hierarchical clustering

mRNAs were obtained from biological replicates of H9 hES cells (n=3), HepaRG-SP (n=4), HepaRG-Spheres (n=4) and HepaRG cells recovered 4 or 10 days after seeding in standard medium (HepaRG-D4 (n=4) or HepaRG-D10 (n=4), respectively). RNA purity and integrity were evaluated with an Agilent Bioanalyser (Agilent Technologies). Genome-wide expression profiling was performed using the low-input QuickAmp labeling kit and human SurePrint G3 8x60K pangenomic microarrays (Agilent Technologies). Gene expression data were processed using Feature Extraction and GeneSpring software (Agilent Technologies).

The data discussed in this publication have been deposited in NCBI's Gene Expression Omnibus (GEO) and are accessible through Series accession number GSE75752 (http://www.ncbi.nlm.nih.gov/geo/query/acc.cgi?acc=GSE75752).

To determine genes significantly deregulated between all different conditions, a one way ANOVA was performed with a p-value $p<0.001$ and a Fold Change (FC)>4. To determine genes significantly deregulated between Spheres and HepaRG-D10 cells or SP and HepaRG-D10 cells, a t-test (Bonferroni FWER correction) with a $p<0.03$, FC>2 and $p<0.05$, FC>3 was used, respectively. Different fold-changes and p-values were used to obtain a comparable numbers of genes in both conditions. Gene Cluster 3.0 software (Pearson metrics with

Accepted manuscript

centroid distances) was used to cluster the selected genes and conditions and TreeView 1.6 to visualize the clustering.

Gene set enrichment analysis

Gene set enrichment analysis (GSEA) was used to check whether an *a priori* defined set of genes showed statistically significant, concordant differences between two biological states. GSEA was performed by using the Java-tool developed at the Broad Institute (Cambridge, MA, USA). Unsupervised GSEA was done with the whole C2 collection of curated gene sets from the molecular signatures database (MSigDB). Enrichment score (ES) was determined after 1,000 permutations, as previously described(13).

Immunohistochemistry

The study protocol complied with French laws and regulations and was approved by INSERM's Institutional Review Board (number 01-036) in the context of the National Network of Liver Biological Resource Centers. Sample collection was reported to the Ministry of Education and Research (No. DC-2008-338). All the patients provided written informed consent before study entry. Tissue Microarray (TMA) comprises 25 HCC patients and 5 histologically normal livers, all in triplicate as previously described(14). Briefly, TMA construction was done with a MiniCore3 tissue arrayer (Alphelys, France). Five-µm microtome sections were processed for immunohistochemistry with a Discovery XT from Ventana Medical Systems (Roche) slide staining system. Antibodies used were purchased from Santa Cruz: hepatocyte nuclear factor 1β (HNF1B, sc-8986), Prolab: CD44 (20282), Sigma Aldrich: leucine-rich repeat-containing G-protein coupled receptor 5 (LGR5, HPA012530), lunatic fringe homolog (LFNG, AV44923), hyaluronan and proteoglycan link protein 1 (HAPLN1, HPA019105), insulin like growth factor binding protein 5 (IGFBP5,

Accepted manuscript

I7660), indian hedgehog (IHH, AV45230), ProteinTech: PDK4 (12949-1-AP) and ANGPTL4 (18374-1-AP). Stained slides were converted into high-resolution digital data with a NanoZoomer digital slide scanner (Hamamatsu, France). Digital slides were viewed using NDP.view software (Hamamatsu). The signal was independently read by 4 observers (KF, OM, FC and AC) who were blinded to any information. Discrepancies were resolved by consensus reading. A 4-point scale (1-2-3-4) reflecting increasing signal intensity was used. Focal and general expressions of the proteins were considered.

Anticancer drug treatments

Adherent cells or spheres were cultured for 3 days in medium deprived of serum and supplemented with cisplatin (Accord Healthcare France SAS, France) or sorafenib (Interchim, France), alone or in combination with DCA.

HCC patient cohorts

Two independent HCC cohorts referred to as "the Roessler's cohort" (n=247 HCCs, GEO Series accession number GSE14520) and the cancer genome atlas liver hepatocellular carcinoma (TCGA-LIHC, n=210 HCCs) cohort were used in the present study. For the Roessler cohort, raw feature data from GEO were normalized and $\log_2$ intensity expression summary values for each probe set were calculated using Robust Multiarray Average (RMA, packages Affy). Each dataset was assessed for the detection of outliers and inter-array, experiment-related batch effects by principal component analysis and density plots. Because a clear-cut inter-array experiment-related batch effect was observed within GSE14520, this effect was corrected by the COMBAT method (package sva). Then, probes being detected over the background noise in at least one HCC were retained and quantile normalized (package preprocessCore). For the TCGA-LIHC cohort, normalized RNAseq data were

Accepted manuscript

downloaded from the Genomic Data Commons website and the patients were selected according to the method detailed in Desert *et al.* 2017(15). Then, hierarchical cluster analysis were performed with the Ward's method using 1-Pearson correlation as a distance metric, based on the expression of the genes up- or down-regulated in HepaRG-SP or HepaRG-Spheres.

Statistical analysis

Results are expressed as means ± standard deviation (SD). Data were analyzed using Graph Pad Prism software (Version 5.0; Graph Pad, San Diego, CA, USA). The significance was evaluated by Student t-test for comparison of 2 conditions or by one-way ANOVA for comparison between groups.

See Supporting Materials and Methods for further information.

Accepted manuscript

RESULTS

HCC cells can retrodifferentiate to cancer stem cells

Cell phenotypic and functional plasticity is known to promote intra-tumor heterogeneity, which in turn contributes to chemotherapy resistances(16). To gain insight into the role of cell plasticity in chemoresistance, we first performed an unsupervised search for gene expression signatures matching the transcriptomic program of 48h-retrodifferentiated hepatocyte-like cells HepaRG cells to HCC progenitor cells (GSE52989) (Supporting Fig. 1A). GSEA revealed that among the top 50 signatures, 38% were related to solid and hematopoietic tumors, and 17% corresponded to stem cells, including the hES cell signature (Fig. 1A). Thus, CSCs can emerge from highly differentiated hepatocyte-like HCC cells.

To further characterize stemness features of HCC cells, we studied anchorage-independent growth and xenobiotic efflux of HepaRG, BC2, HepG2 and HuH7 HCC cell lines. Culture of the 4 cell lines under non-adherent serum- and epidermal growth factor-free conditions resulted in the formation of 3D spheres (Fig. 1B). Spheres upregulated stem cell markers (OCT4, NANOG, CD90) when compared to cells cultured during the same period in adherent conditions (D10). Interestingly, HepaRG and BC2 cells, which are both able to reversibly differentiate, shared specific features: they formed smaller spheres, upregulated stem cell markers and downregulated levels of hepatocyte makers (albumin, aldolase B) in comparison with HepG2 and HuH7 cells (Fig. 1B). Flow cytometry analysis demonstrated that the HepaRG-progenitor cells included 0.6% of SP cells (Fig. 1C) whereas SP cells accounted only for 0.04% in HuH7 and 0.01% in HepG2 cells. Interestingly, SP cells from the HepaRG cell line were able to differentiate to mature hepatocyte-like and biliary-like cells (Fig. 1D), as attested by cytochrome P450 3A4 and cytokeratin 19 staining, respectively (Supporting Fig. 1B). Lastly, BrdU pulse-chase experiments with 2 rounds of cell division without BrdU

Accepted manuscript

revealed late mitotic figures wherein only one nucleus was BrdU-positive, showing that asymmetric division occurred within the HepaRG-progenitor population (Fig. 1E).

Gene signatures of HepaRG Spheres and SP are related to stemness and HCC with poor prognosis

Among the 4 HCC cell lines studied, HepaRG cells harbored the highest plasticity potential and stemness features. Thus, these cells were selected for transcriptomic analyses. Gene profiles of HepaRG-Spheres (Spheres) and HepaRG-SP cells (SP) were compared to those of hES cells (H9), HepaRG-progenitors (D4) and differentiating HepaRG cells (D10) (Supporting Fig. 1A). We identified 5,866 significantly deregulated genes by one-way ANOVA ($p<0.001$, $FC>4$). Hierarchical clustering of the differentially expressed genes showed 2 main branches classifying the samples according to the degree of stemness (Fig. 2A). One branch included D10 whereas the second one grouped hES cells, SP, Spheres and D4. Interestingly, in this stem/progenitor cluster, the gene profiles of SP and Spheres were closer to the gene profiles of hES cells than that of D4. Accordingly, unsupervised GSEA showed significant enrichment of signatures related to stem cells, hepatoblastoma, cancer recurrence and metastasis in the gene profiles obtained from Spheres and SP compared to D10 (Fig. 2B). Notably, both SP and Sphere signatures discriminated 2 subpopulations of HCC patients within 2 public transcriptomic datasets, consisting of 210 and 247 HCC patients, respectively (Fig. 2C). Patients harboring SP or Sphere signatures had a decreased overall survival (Fig. 2C). They also displayed high serum alpha-fetoprotein (AFP) level, tumor grade, Tumor Node Metastases (TNM), Cancer of the Liver Italian Program (CLIP) and Barcelona Clinic Liver Cancer (BCLC) stages, as well as metastasis signatures (Supporting Table 1). Conversely, these patients showed low rates of periportal-type HCC signature, which highlights well-differentiated, favorable outcome tumors(15). Supervised GSEA

Accepted manuscript

confirmed that the SP and Sphere signatures were negatively and positively correlated with the gene expression signatures defining the periportal-type and STEM-type HCC subclasses, respectively (Figure 2D and Supporting Table 2) described by Desert et al.(15).

Acquisition of stem cell properties involves metabolic reprogramming

To gain more insight into the signaling pathways activated in these HCC stem cells, we compared the gene profiles of Spheres and SP versus D10 (Fig. 3A, Supporting Table 3). Ingenuity pathway analysis (IPA) revealed that top upregulated molecules in Spheres were the pro-inflammatory cytokines IL-11, IL-6, IL-1β, which trigger the retrodifferentiation process and ANGPTL4 known to activate ERK and PI3K/AKT signaling pathways(17). Noteworthy, the main activated networks in both Spheres and SP were ERK and PI3K/AKT pathways while TGFβ and TNFα were the upstream regulators (Fig. 3A, Supporting Fig. 1C-D). Consistent with IPA results, a connectivity map approach identified the inhibitor of PI3K LY-294002 among the top 7 ranked molecules that are likely to reverse the gene expression profile induced during spherogenesis (Supporting Table 4).

Analysis of 788 common genes differentially expressed in Spheres and SP versus D10 ($p<0.05$, $FC>2$) performed by GSEA confirmed significant enrichment of signatures related to stem cells, inflammatory response, angiogenesis and tumorogenesis, in both Spheres and SP (Fig. 3B, Supporting Tables 5-6). Besides activation of ERK and PI3K, IPA identified peroxisome proliferator-activated receptor γ (PPARG) and PPARG coactivator 1α (PPARGC1A) associated to downregulation of numerous genes involved in the tricarboxylic acid (TCA) and OXPHOS. Decreased expression of *PPARGC1A*, known as a nodal regulator of mitochondria biogenesis and function, could be related to changes in mitochondrial pathways in both Spheres and SP cells (Fig. 3B). A downregulation of genes involved in OXPHOS [*cytochrome c oxidase* (*COX), NADH:Ubiquinone Oxidoreductase* (*NDUF),*

Accepted manuscript

succinate dehydrogenase (SDH) and *ubiquinol cytochrome c oxidoreductase chain (UQRC)* families] was also observed with concurrent upregulation of glucose transporters (*GLUT3, 5* and *6*) and glycolytic enzymes [*Phosphofructokinase, Platelet (PFKP), pyruvate kinase M (PKM*)] (Fig. 3C and Supporting Fig. 1E). Moreover, poor labeling of mitochondria by Mitotracker® red revealed a reduced mitochondrial membrane potential in SP compared to non-SP (NSP) cells, and suggested a reduced mitochondrial activity although the mitochondrial mass, assessed with COX subunit II (COX2) staining, was higher (Fig. 3D). Lower mitochondrial membrane potential was associated with lipid accumulation in Spheres and SP (Fig. 3E). In parallel to PPARGC1A decrease, upregulation of PPARG was associated with increased transcription of its target gene PDK4, an inhibitor the pyruvate dehydrogenase (PDH) complex (Fig. 3C). In keeping with the role of PDK4, increased phosphorylation of the E1-α subunit of PDH complex, high lactate production, low pyruvate consumption and low ATP content were observed in HepaRG-Spheres (Fig. 3F). Of note, due to the limited number of available SP cells, the later experiments were only performed on Spheres.

Upregulated expression of ANGPTL4 and PDK4 is associated with stem cell markers in human HCCs

Unlike most other genes related to cell metabolism that were repressed, *ANGPTL4* and *PDK4* were found highly upregulated in HepaRG-Spheres and –SP (Fig 3C). Interestingly, both were also significantly upregulated in BC2-Spheres along with stem cell markers (Fig. 1C, Supporting Fig. 1F). This prompted us to evaluate the expression of ANGPTL4 and PDK4 by TMA-based immunochemistry in human HCCs (n=25) and normal livers (n=5). In normal liver, ANGPTL4 and PDK4 were predominantly detected in the cytoplasm of hepatocytes (Supporting Fig. 1G). In HCCs, ANGPTL4 and PDK4 showed similar staining patterns: both proteins were diffusely detected in the tumor (Fig. 4A, Supporting Fig. 1H). However,

Accepted manuscript

scattered cells showing upregulated expression of ANGPTL4 and PDK4 could be observed within the tumor parenchyma and intra-tumor fibrous tracts. Immunostaining of serial sections showed a similar staining pattern with respect to the progenitor/stem cell markers CD44, LGR5, HNF1B, IHH, LFNG, IGFBP5 and HAPLN1 (Fig. 4B, Supporting Fig. 1H). Of note, ANGPTL4/PDK4-positive cells located within intra-tumor fibrous tracts were positive for anti-hepatocyte antibody (Supporting Fig. 1H). *In situ* protein expression was semi-quantitatively rated on a 4-point scale (1-4) by 4 observers in 25 HCCs. ANGPTL4 and PDK4 scores were highly correlated (Fig. 4C, Supporting Fig. 1I) and associated with CSC markers, as shown by network correlation analysis (Fig. 4D). In addition, HCCs without tumor necrosis showed high protein expression scores of ANGPTL4 and PDK4 (Fig. 4E).

ANGPTL4 knockdown alters anti-inflammatory response, angiogenesis and tumor cell invasion

ANGPTL4 is a multifaceted secreted protein that could play a role in anoikis resistance by stimulating NADPH oxidase, therefore leading to activation of the ERK and PI3K pro-survival pathways. In agreement, we found in Spheres and SP cells increased expression of the integrin β1 subunit ITGB1, which is known to bind ANGPTL4 and transduce its signal (17) (Supporting Fig. 1J). Hence, to evaluate the role of ANGPTL4 on stemness acquisition and metabolism adaptation, we performed loss-of-function experiments in HepaRG cells only using Spheres, because the limited number of available SP cells did not allow us to carry out concomitant analyses. Transduction with lentivirus encoding shRNA against ANGPTL4 (ShANGPTL4) greatly diminished synthesis and secretion of ANGPTL4 whereas it neither affected spherogenesis nor viability assessed by lactate dehydrogenase (LDH) release (Fig. 5A-B). ANGPTL4 knockdown reduced ERK phosphorylation, slightly decreased PI3K expression whereas phosphorylated AKT was increased (Fig. 5A). Concomitantly, we

Accepted manuscript

detected a downregulated expression of metalloproteinases (MMP) MMP2, MMP13, anti-inflammatory cytokine IL-11 and pro-angiogenic factor vascular endothelial growth factor A (VEGF) (Fig. 5C). These observations were consistent with reduced invasion capacity of the ShANGPTL4-Spheres (Fig. 5D). In metabolic terms, pyruvate and lactate extracellular concentrations as well as ATP and lipids contents were unchanged (Fig. 5E and Supporting Fig. 1K). Interestingly, downregulation of PDK4 by ShANGPTL4 (Fig. 5C) may favor mitochondrial activity as suggested by higher the MitoTracker® staining (Fig. 5F). In contrast, COX2 staining was decreased by ShANGPTL4, thus suggesting that the compensatory increase in mitochondrial mass was no longer required for the restoration of mitochondrial activity.

ERK inhibition reduces cell invasion properties and PI3K inhibition alters cell survival

To specify the role of ERK and PI3K, downstream effectors of ANGPTL4/integrin signaling, we sought to target both pathways, which were found strongly activated in Spheres, using specific inhibitors. Although the sphere number was reduced and mild cell toxicity was detected by higher LDH release in the culture medium, HepaRG-progenitors treated with the MEK1/2 inhibitor U0126 (10µM) preserved their spherogenesis ability (Fig. 6A). After treatment, ERK phosphorylation was markedly reduced whereas the total amount of ERK was unchanged (Fig. 6A). Unlike *OCT4 and NANOG*, mRNA levels of *ANGPTL4, PDK4, VEGF, IL-6, IL-11, MMP1, 2, 9* and *13* were decreased by U0126 (Fig. 6B). Consistent with the sharp downregulation of MMPs, a strong inhibition of the invasive potential of the spheres was observed (Fig. 6C). The ATP content was decreased, concomitantly to cell viability, while the lactate and pyruvate extracellular concentrations were not modified (Fig. 6D).

HepaRG-progenitors treated with the PI3K inhibitor LY294002 (10µM) showed an inhibition of AKT phosphorylation that resulted in alteration of sphere formation. Moreover, the release

Accepted manuscript

of LDH during the culture revealed reduced cell viability (Fig. 6E). In remaining cells, RNA levels of *ANGPTL4, PDK4, VEGF, IL-6, IL-11, PDK4, MMP1, 2, 9* and *13* were downregulated compared to those of untreated spheres whereas *OCT4* and *NANOG* expression was unchanged (Fig. 6F). Of note, 10µM LY294002 did not affect HepaRG-D10 cell viability. The low number of viable cells after LY294002 treatment did not allow us to perform metabolism and invasion assays.

PDK4 inhibition combined with chemotherapy increases tumor cell death

Since *ANGPTL4* and *PDK4* were found upregulated in stem/progenitor cells, we investigated their possible involvement in the resistance to standard chemotherapies. When exposed to cisplatin or sorafenib for 3 days, the viability of HepaRG, BC2, HuH7 and HepG2 cells was reduced by 50 to 80% compared to untreated cells. In contrast, HepaRG- and BC2-Spheres were totally chemoresistant. However, a moderate efficacy of cisplatin could be noted against HepG2- and HuH7-Spheres (Fig. 7A). Interestingly, in HepaRG-D4 cells that were resistant to cisplatin or sorafenib, we observed an increased expression of *OCT4, NANOG, ANGPTL4* and *PDK4* (Fig. 7B). Moreover, among these markers, PDK4 expression was found significantly increased in all HCC Spheres (Supporting Fig. 1F). Hence, we hypothesized that inhibition of PDK4 could reduce the chemoresistance by reactivating the mitochondrial PDH complex. Accordingly, in ShANGPTL4-HepaRG-Spheres, reduced expression of PDK4 sensitized cells to sorafenib (Fig. 7C). Therefore, we evaluated the effects of the chemical PDK inhibitor DCA against HCC cell lines. DCA (50mM) induced drastic decrease in cell viability in HepaRG-Spheres, which expressed the highest levels of PDK4 (Fig. 7B-C, Supporting Fig. 1F) and the co-treatment DCA/chemotherapy did not provide significant additional effect. Low expression levels of antioxidant enzymes such as *hemoxygenase2 (HMOX2), superoxide dismutase 1* and *3* (*SOD1* and *3*), and *glutathione peroxidase 1* and *4*

Accepted manuscript

(*GPX1* and *4*) in HepaRG-Spheres (Supporting Fig. 1L) may enhance reactive oxygen species (ROS) toxicity and contribute to efficacy of DCA alone (Fig. 7C). On the contrary, DCA had no effect on cell viability of HepaRG-D10 and showed mild efficiency on HepaRG-D4, which expressed low and intermediate PDK4 levels, respectively. Knocking-down PDK4 expression with siRNA in HepaRG-D4 also reduced cell viability (Fig. 7C and Supporting Fig. 1M). Co-treatment DCA/chemotherapy was more effective than chemotherapy alone on both HepaRG-D4 and HepaRG-D10 (Fig. 7C). In addition, efficacy of DCA and co-treatment DCA/chemotherapy was confirmed in BC2, HepG2 and HuH7 HCC cell lines (Fig. 7C) that all expressed PDK4 at various levels (Supporting Fig. 1F).

Accepted manuscript

DISCUSSION

Cell heterogeneity is one of the main features of HCC and likely contributes to drug resistance. The tumor microenvironment can significantly influence cell fate. Therefore, by understanding the mechanisms underlying how tumor cells adapt to their environment, the molecular basis of chemoresistance may be understood. We previously demonstrated that the crosstalk between the pro-inflammatory cytokines TNFα, IL-6, and TGFβ triggers retrodifferentiation of hepatocyte-like HCC cells into proliferating liver progenitors whose gene signatures match proliferative HCC subclasses that have a poor prognosis(4). In this work, we show that liver progenitors retrodifferentiate towards even more immature cells endowed with stem properties and increased chemoresistance. Both Spheres and SP expressed gene signatures related to stemness, inflammation, HCC metastasis and recurrence. Notably, HCCs expressing the Sphere or SP signatures were associated with unfavorable outcome.

Gene expression profiling revealed that cytokines (TNFα, IL-6, TGFβ, IL-11), whose expression in HCCs are associated with poor prognosis(18-21) and involved in retrodifferentiation, were expressed in Spheres and SP at higher levels than in progenitor cells. This emphasizes the role of an autocrine regulation by cytokines in cell fate conversion within the tumor and the maintenance of stem cell properties. It also highlights that the acquisition of stem properties was associated with an important modulation in cell metabolism. To support these findings, among the upregulated genes in both Spheres and SP, we identified ANGPTL4, a molecule described as a potential modulator of the cross-talk between metabolism and cancer(22), and PDK4, an enzyme responsible of cell metabolic plasticity(23).

ANGPTL4 is a circulating protein predominantly produced in the liver and adipose tissue, that regulates lipid and carbohydrate metabolism, redox homeostasis and attenuates the inflammatory response(24). The biological significance of ANGPTL4 in cancer remains

Accepted manuscript

controversial. In the liver, ANGPTL4 expression has been found to be associated with cancer cell extravasation, enhanced tumorigenesis and poor prognosis(25). In HCC patients, serum ANGPTL4 levels correlate with tumor progression and metastasis(25,26). In contrast, ANGPTL4 expression has been shown to be significantly lower in HCC tissue than in non-tumor tissue. The downregulation of ANGPTL4 RNA levels has been associated with advanced tumor stage, high alpha-fetoprotein levels, poor differentiation and tumor recurrence(27,28). Furthermore, ANGPTL4 may suppress HCC progression and metastasis in mice through disruption of a tumor-favorable microenvironment(27). This discrepancy may result from the dual expression pattern of ANGPTL4 in human HCCs. Using immunohistochemistry, we observed a diffuse staining pattern of variable intensity in the tumor hepatocyte cytoplasm but also a very strong signal in scattered cells expressing CSC markers within the tumor parenchyma and intra-tumor fibrous tracts. The hypothesis that ANGPTL4 is involved in malignant progression was supported by *in vitro* knock-down of ANGPTL4 in HCC cells expressing CSC features.

ANGPTL4 expression was able to regulate IL-11 but not IL-6 production. Initially considered as an anti-inflammatory cytokine promoting cell adaptation to inflammatory environment, IL-11 has been recently reported to present pro-tumorigenic properties by protecting epithelial cells from death(29) and activating oncogenic signaling pathways(30). By interacting with integrins (predominantly ITGB1 and ITGB5), tumor-derived ANGPTL4 also sustains anchorage-related signals in the absence of extracellular matrix and cell-cell contacts. It stimulates NADPH oxidase-dependent production of ROS to maintain a high anion superoxide ($O_2^{\cdot-}$)/hydrogen peroxide (H_2O_2) ratio that activates the ERK and PI3K pro-survival pathways(17). We demonstrated that ANGPTL4 contributes to ERK activation and PI3K signalling, leading to upregulation of MMP-2 and 13 allowing tumor invasion and VEGF-A allowing angiogenesis. We also confirmed that PI3K/AKT and ERK signalling

Accepted manuscript

pathways are crucial for cell survival, inflammatory response, while stem cell marker expression was unchanged.

The PPARγ, TGFβ and HIF1α pathways are able to induce ANGPTL4 expression(22,31). In the small HepaRG-Spheres (less than 200μm diameter), no significant accumulation of HIF1α was detected (Supporting Fig. 1N). In addition, high protein expression scores of ANGPTL4 were found in human HCCs without tumor necrosis, suggesting that tumors enriched in stem/progenitor cells are metabolically fit to withstand the cancer microenvironment. In terms of PPARγ and TGFβ signalling, they are both activated in Spheres and SP, and also described to regulate PDK4 expression(32,33). In addition, we observed that inhibition of ERK or PI3K, known to affect PPARγ transcriptional activity(34), decreased both ANGPTL4 and PDK4 expression.

Silencing ANGPTL4 in Spheres also decreased PDK4 expression and increased mitochondrial membrane potential, emphasizing its potential role in mediating an interplay between inflammation, metastasis and metabolism(22). The PDH complex manages the competition between glucose and fatty acid oxidation by controlling the conversion of pyruvate into acetyl-coenzyme A. Therefore, by inactivating the PDH complex, PDK4 plays a pivotal role in metabolic plasticity since it restricts the supply of acetyl-coenzyme A from glucose oxidation to feed the TCA cycle. We noted low pyruvate consumption and high lactate production in the HepaRG-Spheres. However, reduced OXPHOS gene expression, mitochondrial ATP synthesis and membrane potential, associated with accumulation of lipids suggested a lack of metabolic switch toward long chain-fatty acid oxidation to feed the TCA cycle. ANGPTL4 has been shown to inhibit lipoprotein lipase activity and contributes to intracellular lipase degradation (35,36). The increased expression of phosphofructokinase and glucose transporters GLUT3, 5 and 6 combined with the decreased expression of

Accepted manuscript

PPARGC1A, a nodal regulator of mitochondrial biogenesis and function, suggest that both SP and Spheres use preferably the glycolytic pathway.

Mitochondria are the primary cellular source of ROS, in particular $O_2^{\cdot-}$, which is readily dismutated to the freely diffusible and cytotoxic H_2O_2(37). Therefore, a reduction in OXPHOS could favor the survival of stem cells as a result of decreased mitochondrial H_2O_2 release(38). In addition, decreased mitochondrial activity is expected to impair the intrinsic apoptotic pathway(39). Consistent with these observations, metabolism reprogramming associated with a glycolytic profile is observed in hES and induced pluripotent stem cells, which leads to lower levels of ROS than in their progeny(40). During somatic reprogramming to pluripotency, it was demonstrated that glycolytic shift and inhibition of pyruvate transport into mitochondria occurs as a consequence of the induction of the expression of mitochondrial enzyme PDK1, which inhibits PDH(41). In the same way, recent reports suggest that a decrease in gene expression and protein amounts of the PDH complex in breast tumor-initiating cells is linked to reduced mitochondrial activity and higher glycolysis(42). A more active glycolysis over OXPHOS was detected in the$CD133^+$ PLC/PRF/5 human HCC cell line compared to $CD133^-$ cells(43) and in liver tumor-initiating stem-like cells in mice(44).

Recently, reports have suggested a causal link between metabolic change or mitochondrial dysfunction and chemoresistance. Consistent with this hypothesis, HCC-Spheres were resistant to cisplatin and sorafenib treatments compared to adherent cultures. The greatest cisplatin resistance of HepaRG and BC2 compared to HuH7 and HepG2 Spheres may result from the presence of proliferative cells in high-growing HuH7 and HepG2 Spheres. Moreover, HepaRG-D4 resistant cells strongly expressed OCT4, NANOG, ANGPTL4 and PDK4. These data suggest that these drugs spare cells with stem cell characteristics. Importantly, DCA, which is known to redirect glucose metabolism from glycolysis to TCA and OXPHOS(38), succeeded in increasing the effect of chemotherapies against all HCC cell

Accepted manuscript

lines assessed. The chemotherapeutic effect of DCA may originate from the inability of cells to counteract the increased ROS production following mitochondria reactivation. This effect was especially notable in Spheres, probably because of their low levels of antioxidant enzymes.

Despite initial favorable responses with sorafenib and improved survival with regorafenib(45), tyrosine kinase inhibitors do not completely block HCC progression(46-48). Therefore, identifying new therapeutic targets remains a challenge. We have demonstrated that cisplatin and sorafenib resistant HCC cells exhibit stem cells properties and have revealed that ANGPTL4/PDK4 contribute to the maintenance of CSC features. Importantly, we provide the proof of concept that targeting the enzymes involved in metabolic reprogramming could be useful in association with chemotherapy to better control HCC recurrence.

Accepted manuscript

ACKNOWLEDGEMENTS

The authors thank Drs. P. Loyer and C. Aninat for thoughtful discussions and critical reading of the manuscript, Drs. L. Sulpice and D. Bergeat, Rennes University Hospital, for patient data, Drs. Mireille Desille and Bruno Turlin, CRB-Santé, Biosit, Biogenouest, Rennes, France. The authors also thank the "Genomique Santé", "ImPACcell", "flow cytometry", "H2P2" Core facilities from Biogenouest, SFR Biosit, University of Rennes1 and the "flow cytometry" Core facility from Paul Brousse Hospital, Villejuif.

This work was supported by the Institut National de la Santé et de la Recherche Médicale (BF, OM, DG, CR), the Centre National de la Recherche Scientifique (AC), the University of Rennes 1 (FC, YD), the « association pour la recherche sur le cancer », the «Ligue contre le cancer - Comités d'Ille-et-Vilaine, des Côtes d'Armor, de Loire Atlantique et de Vendée», Cancéropôle Grand Ouest (CONCERTO) and Institut National du Cancer (Grant n°12688). KF was funded by the «Conseil Régional de Bretagne», INSERM (CESOCA) and the Ligue contre le cancer-Comité d'Ille et Vilaine. HDPS was funded by the Seventh Framework Programme (FP7) LIV-ES (Grant n°223317) and the «Contrat Plan Etat-Région». RD was funded by the «Conseil Régional de Bretagne» and INSERM (VALCIPRE).

Accepted manuscript

REFERENCES

1. Marquardt JU, Andersen JB, Thorgeirsson SS. Functional and genetic deconstruction of the cellular origin in liver cancer. Nature reviews **2015**;15:653-67
2. Roskams T. Liver stem cells and their implication in hepatocellular and cholangiocarcinoma. Oncogene **2006**;25:3818-22
3. Holczbauer A, Factor VM, Andersen JB, Marquardt JU, Kleiner DE, Raggi C*, et al.* Modeling pathogenesis of primary liver cancer in lineage-specific mouse cell types. Gastroenterology **2013**;145:221-31
4. Dubois-Pot-Schneider H, Fekir K, Coulouarn C, Glaise D, Aninat C, Jarnouen K*, et al.* Inflammatory cytokines promote the retrodifferentiation of tumor-derived hepatocyte-like cells to progenitor cells. Hepatology (Baltimore, Md **2014**;60:2077-90
5. Tarlow BD, Pelz C, Naugler WE, Wakefield L, Wilson EM, Finegold MJ*, et al.* Bipotential adult liver progenitors are derived from chronically injured mature hepatocytes. Cell stem cell **2014**;15:605-18
6. Cabillic F, Corlu A. Regulation of Transdifferentiation and Retrodifferentiation by Inflammatory Cytokines in Hepatocellular Carcinoma. Gastroenterology **2016**;151:607-15
7. Hadnagy A, Gaboury L, Beaulieu R, Balicki D. SP analysis may be used to identify cancer stem cell populations. Experimental cell research **2006**;312:3701-10
8. Oishi N, Yamashita T, Kaneko S. Molecular biology of liver cancer stem cells. Liver cancer **2014**;3:71-84
9. Martinez-Outschoorn UE, Peiris-Pages M, Pestell RG, Sotgia F, Lisanti MP. Cancer metabolism: a therapeutic perspective. Nat Rev Clin Oncol **2017**;14:11-31
10. Sancho P, Barneda D, Heeschen C. Hallmarks of cancer stem cell metabolism. Br J Cancer **2016**;114:1305-12
11. Glaise D, Ilyin GP, Loyer P, Cariou S, Bilodeau M, Lucas J*, et al.* Cell cycle gene regulation in reversibly differentiated new human hepatoma cell lines. Cell Growth Differ **1998**;9:165-76
12. Cerec V, Glaise D, Garnier D, Morosan S, Turlin B, Drenou B*, et al.* Transdifferentiation of hepatocyte-like cells from the human hepatoma HepaRG cell line through bipotent progenitor. Hepatology (Baltimore, Md **2007**;45:957-67
13. Coulouarn C, Corlu A, Glaise D, Guenon I, Thorgeirsson SS, Clement B. Hepatocyte-stellate cell cross-talk in the liver engenders a permissive inflammatory microenvironment that drives progression in hepatocellular carcinoma. Cancer research **2012**;72:2533-42
14. Mebarki S, Desert R, Sulpice L, Sicard M, Desille M, Canal F*, et al.* De novo HAPLN1 expression hallmarks Wnt-induced stem cell and fibrogenic networks leading to aggressive human hepatocellular carcinomas. Oncotarget **2016**;7:39026-43
15. Desert R, Rohart F, Canal F, Sicard M, Desille M, Renaud S*, et al.* Human hepatocellular carcinomas with a periportal phenotype have the lowest potential for early recurrence after curative resection. Hepatology (Baltimore, Md **2017**;66:1502-18
16. Friemel J, Rechsteiner M, Frick L, Bohm F, Struckmann K, Egger M*, et al.* Intratumor heterogeneity in hepatocellular carcinoma. Clin Cancer Res **2015**;21:1951-61
17. Zhu P, Tan MJ, Huang RL, Tan CK, Chong HC, Pal M*, et al.* Angiopoietin-like 4 protein elevates the prosurvival intracellular O2(-):H2O2 ratio and confers anoikis resistance to tumors. Cancer cell **2011**;19:401-15
18. Nong Y, Wu D, Lin Y, Zhang Y, Bai L, Tang H. Tenascin-C expression is associated with poor prognosis in hepatocellular carcinoma (HCC) patients and the inflammatory

Accepted manuscript

cytokine TNF-alpha-induced TNC expression promotes migration in HCC cells. Am J Cancer Res **2015**;5:782-91
19. Ohishi W, Cologne JB, Fujiwara S, Suzuki G, Hayashi T, Niwa Y*, et al.* Serum interleukin-6 associated with hepatocellular carcinoma risk: a nested case-control study. Int J Cancer **2014**;134:154-63
20. Lin TH, Shao YY, Chan SY, Huang CY, Hsu CH, Cheng AL. High Serum Transforming Growth Factor-beta1 Levels Predict Outcome in Hepatocellular Carcinoma Patients Treated with Sorafenib. Clin Cancer Res **2015**;21:3678-84
21. Xiang ZL, Zeng ZC, Fan J, Tang ZY, Zeng HY. Expression of connective tissue growth factor and interleukin-11 in intratumoral tissue is associated with poor survival after curative resection of hepatocellular carcinoma. Molecular biology reports **2012**;39:6001-6
22. La Paglia L, Listi A, Caruso S, Amodeo V, Passiglia F, Bazan V*, et al.* Potential Role of ANGPTL4 in the Cross Talk between Metabolism and Cancer through PPAR Signaling Pathway. PPAR Res **2017**;2017:8187235
23. Zhang S, Hulver MW, McMillan RP, Cline MA, Gilbert ER. The pivotal role of pyruvate dehydrogenase kinases in metabolic flexibility. Nutr Metab (Lond) **2014**;11:10
24. Zhu P, Goh YY, Chin HF, Kersten S, Tan NS. Angiopoietin-like 4: a decade of research. Bioscience reports **2012**;32:211-9
25. Li H, Ge C, Zhao F, Yan M, Hu C, Jia D*, et al.* Hypoxia-inducible factor 1 alpha-activated angiopoietin-like protein 4 contributes to tumor metastasis via vascular cell adhesion molecule-1/integrin beta1 signaling in human hepatocellular carcinoma. Hepatology (Baltimore, Md **2011**;54:910-9
26. El-Shal AS, Zidan HE, Rashad NM, Wadea FM. Angiopoietin-like protein 3 and 4 expression 4 and their serum levels in hepatocellular carcinoma. Cytokine **2017**;96:75-86
27. Ng KT, Xu A, Cheng Q, Guo DY, Lim ZX, Sun CK*, et al.* Clinical relevance and therapeutic potential of angiopoietin-like protein 4 in hepatocellular carcinoma. Molecular cancer **2014**;13:196
28. Zhang H, Wei S, Ning S, Jie Y, Ru Y, Gu Y. Evaluation of TGFbeta, XPO4, elF5A2 and ANGPTL4 as biomarkers in HCC. Experimental and therapeutic medicine **2013**;5:119-27
29. Putoczki T, Ernst M. More than a sidekick: the IL-6 family cytokine IL-11 links inflammation to cancer. Journal of leukocyte biology **2010**;88:1109-17
30. Onnis B, Fer N, Rapisarda A, Perez VS, Melillo G. Autocrine production of IL-11 mediates tumorigenicity in hypoxic cancer cells. The Journal of clinical investigation **2013**;123:1615-29
31. Padua D, Zhang XH, Wang Q, Nadal C, Gerald WL, Gomis RR*, et al.* TGFbeta primes breast tumors for lung metastasis seeding through angiopoietin-like 4. Cell **2008**;133:66-77
32. Strand DW, Jiang M, Murphy TA, Yi Y, Konvinse KC, Franco OE*, et al.* PPARgamma isoforms differentially regulate metabolic networks to mediate mouse prostatic epithelial differentiation. Cell death & disease **2012**;3:e361
33. Zhang Y, Zhang Y, Geng L, Yi H, Huo W, Talmon G*, et al.* Transforming Growth Factor beta Mediates Drug Resistance by Regulating the Expression of Pyruvate Dehydrogenase Kinase 4 in Colorectal Cancer. The Journal of biological chemistry **2016**;291:17405-16
34. Chen L, Necela BM, Su W, Yanagisawa M, Anastasiadis PZ, Fields AP*, et al.* Peroxisome proliferator-activated receptor gamma promotes epithelial to

Accepted manuscript

mesenchymal transformation by Rho GTPase-dependent activation of ERK1/2. The Journal of biological chemistry **2006**;281:24575-87
35. Dijk W, Beigneux AP, Larsson M, Bensadoun A, Young SG, Kersten S. Angiopoietin-like 4 promotes intracellular degradation of lipoprotein lipase in adipocytes. J Lipid Res **2016**;57:1670-83
36. Dijk W, Kersten S. Regulation of lipid metabolism by angiopoietin-like proteins. Curr Opin Lipidol **2016**;27:249-56
37. Tahara EB, Navarete FD, Kowaltowski AJ. Tissue-, substrate-, and site-specific characteristics of mitochondrial reactive oxygen species generation. Free radical biology & medicine **2009**;46:1283-97
38. Bonnet S, Archer SL, Allalunis-Turner J, Haromy A, Beaulieu C, Thompson R, *et al.* A mitochondria-K+ channel axis is suppressed in cancer and its normalization promotes apoptosis and inhibits cancer growth. Cancer cell **2007**;11:37-51
39. Green DR, Kroemer G. The pathophysiology of mitochondrial cell death. Science (New York, NY **2004**;305:626-9
40. Prigione A, Ruiz-Perez MV, Bukowiecki R, Adjaye J. Metabolic restructuring and cell fate conversion. Cell Mol Life Sci **2015**
41. Varum S, Rodrigues AS, Moura MB, Momcilovic O, Easley CAt, Ramalho-Santos J, *et al.* Energy metabolism in human pluripotent stem cells and their differentiated counterparts. PloS one **2011**;6:e20914
42. Feng W, Gentles A, Nair RV, Huang M, Lin Y, Lee CY, *et al.* Targeting unique metabolic properties of breast tumor initiating cells. Stem cells (Dayton, Ohio) **2014**;32:1734-45
43. Song K, Kwon H, Han C, Zhang J, Dash S, Lim K, *et al.* Active glycolytic metabolism in CD133(+) hepatocellular cancer stem cells: regulation by MIR-122. Oncotarget **2015**;6:40822-35
44. Chen CL, Uthaya Kumar DB, Punj V, Xu J, Sher L, Tahara SM, *et al.* NANOG Metabolically Reprograms Tumor-Initiating Stem-like Cells through Tumorigenic Changes in Oxidative Phosphorylation and Fatty Acid Metabolism. Cell metabolism **2016**;23:206-19
45. Kim K, Jha R, Prins PA, Wang H, Chacha M, Hartley ML, *et al.* Regorafenib in advanced hepatocellular carcinoma (HCC): considerations for treatment. Cancer Chemother Pharmacol **2017**;80:945-54
46. Llovet JM, Decaens T, Raoul JL, Boucher E, Kudo M, Chang C, *et al.* Brivanib in patients with advanced hepatocellular carcinoma who were intolerant to sorafenib or for whom sorafenib failed: results from the randomized phase III BRISK-PS study. J Clin Oncol **2013**;31:3509-16
47. Cheng AL, Kang YK, Lin DY, Park JW, Kudo M, Qin S, *et al.* Sunitinib versus sorafenib in advanced hepatocellular cancer: results of a randomized phase III trial. J Clin Oncol **2013**;31:4067-75
48. Bruix J, Qin S, Merle P, Granito A, Huang YH, Bodoky G, *et al.* Regorafenib for patients with hepatocellular carcinoma who progressed on sorafenib treatment (RESORCE): a randomised, double-blind, placebo-controlled, phase 3 trial. Lancet **2017**;389:56-66

Accepted manuscript

FIGURE LEGENDS

Figure 1: Characterization of stem cell features in HCC cell lines.

(A) Unsupervised GSEA using the gene expression profiles of mature HepaRG-hepatocyte-like cells before and after 48 hours of retrodifferentiation. Top 50 gene signatures identified by GSEA (left panel).Among them GSEA revealed an enrichment of stem signatures such as the "Benporath_ES Signature" related to genes overexpressed in human embryonic stem cells (right panel). (B) Phase-contrast photographs of HepaRG, BC2, HepG2 and HuH7 Spheres. Bar=50µm. mRNA levels of OCT4, NANOG, CD90, albumin and aldolase B in HepaRG, BC2, HepG2 and HuH7 Spheres (Spheres) compared to 10 day-old cells cultured in adherent conditions (D10) (n=3). *p<0.05, **p<0.01, ***p<0.001. (C) Flow cytometry showing the HepaRG-SP population (SP) that efficiently effluxes the Hoechst 33342 dye. (D) Phase-contrast photographs of sorted SP and unsorted HepaRG cells at D4, D8, D15, D20, D30 and D35 after plating. Bar=50µm. (E) BrdU and Hoechst stainings in HepaRG progenitors (HepaRG-D4) after BrdU-pulse chase experiment. Bar=10µm.

Figure 2: SP and Sphere signatures match with poor outcome in HCC.

(A) Filtered microarray data clustered with Gene Cluster 3.0 and visualized with Treeview; SP: HepaRG-side population, Spheres: HepaRG-Spheres, D4: HepaRG-D4 (progenitors), D10: HepaRG-D10; H9: human Embryonic Stem cells. Green indicates lower expression; red higher expression. (B) Unsupervised GSEA highlighted enrichment of stem cell, hepatoblastoma, metastasis and cancer recurrence signatures in HepaRG-SP and HepaRG-Spheres compared to HepaRG-D10 cells: Lim_mammary_stem_cell_up, Pece_mammary_stem_cell_up, Cairo_hepatoblastoma_up, Hoebeke_lymphoid_stem_cell_up, Liao_metastasis and Woo_liver_cancer_recurrence_up signatures. (C) Hierarchical clustering of patients from the Roessler cohort (GSE14520) and TCGA-LIHC cohort on the basis of SP

Accepted manuscript

or Sphere mRNA expression signature. Analysis was performed using the Ward's method using 1-Pearson correlation as a distance metric, based on the differential expression of the genes regulated in SP or Spheres (red) in comparison to HepaRG-D10 (blue). Kaplan-Meier curves for overall survival. Red curves: patients harboring SP or Sphere signature. (D) GSEA showed that the gene profiles in SP and Spheres were enriched in gene signature corresponding to Desert_liver_subclass_stem and depleted in gene signature corresponding to Desert_liver_subclass_PP.

Figure 3: Acquisition of stem cell properties and metabolic adaptation in HepaRG cells.
(A) Number of significantly deregulated genes between HepaRG-Spheres (Spheres) and HepaRG-D10 cells (D10) ($p<0.03$, $FC>2$), and between HepaRG-SP (SP) and D10 ($p<0.05$, $FC>3$). Networks, top up- or down-regulated molecules, top upstream regulators highlighted by IPA. (B) Venn diagram showing common genes between Spheres and SP both compared to D10. Numbers of common up- or down-regulated genes in SP and Spheres ($p<0.05$, $FC>2$). Top canonical pathways, networks, upstream regulators and top regulator effect networks highlighted by IPA. (C) Heatmap of key genes involved in glycolysis, tricarboxylic acid cycle (TCA) cycle and mitochondrial enzymes in SP, Spheres and D10. Upregulation is represented by red shading; downregulation is represented by green shading. (D) COX2 and MitoTracker® staining in SP and non-SP (NSP) cells and quantification by Cell Health Profiling (Cellomics, n=3). Bar=50µm. (E) Oil-Red O staining in Spheres, D10, SP and NSP cells. Bar=50µm. (F). Levels of lactate, pyruvate and ATP in Spheres and D10. ATP content is expressed as relative to D10 and is arbitrary set to 1 (n=3). Relative expression of PDHA1 in HepaRG-Spheres and HepaRG-D10. Western blot showing levels of PDHE1A and P-S293-PDHE1A in HepaRG-Spheres and D10. *$p<0.05$, **$p<0.01$, ***$p<0.001$.

Accepted manuscript

Figure 4: Association of ANGPTL4 and PDK4 expression with stem/progenitor cell markers in human HCCs. (A-C) Tissue-microarray-based immunostainings in HCCs. (A) Serial sections showed similar staining patterns for ANGPTL4 and PDK4. Homogeneous staining coexisted with scattered tumor cells showing higher intensity signal *(arrowheads)*. (B) Serial sections of a same HCC wherein homogeneous staining coexisted with scattered tumor cells showing higher intensity signal for ANGPTL4, PDK4, CD44, LGR5, IHH, LFNG, IGFBP5 and HAPLN1 *(arrowheads)*. HNF1B staining highlighted tumor cell cords infiltrating the tumor extracellular matrix *(arrowheads)*. (C) Immunostaining was quantified on a 0-4 scale by two observers. Protein expression scores of ANGPTL4 and PDK4 were correlated in 25 HCCs. Bars indicate mean±SD. (D) Cytoscape correlation network analysis of the nine proteins based on a Gamma correlation coefficient value matrix (Supporting Fig. 3B). Statistically significant coefficients ($p<0.05$; $r \geq 0.4$) are represented by red links between nodes. Link color intensity and thickness are proportional to correlation coefficients. (E) ANGPTL4 and PDK4 tumor scores were higher in HCCs without (n=12) than with (n=13) tumor necrosis (Student's *t* test). Bars indicate mean±SD.

Figure 5: Involvement of ANGPTL4 in inflammation, angiogenesis and invasion in HepaRG cells.

(A) Phase-contrast photographs of non-targeting ShRNA (ShNTC) or ShANGPTL4 Spheres. Bar=50µm. Western blot showing levels of ANGPTL4, ERK, P-ERK, PI3K, AKT and P-AKT in ShNTC and ShANGPTL4 Spheres. (B) Secretion of ANGPTL4 determined by ELISA in ShNTC and ShANGPTL4 Spheres. Number of Spheres after seeding of 100,000 ShNTC- or ShANPTL4-infected cells. Viability of ShNTC and ShANGPTL4 Spheres assessed by LDH release (n=3). (C) mRNA levels of OCT4, NANOG, IL-6, IL-11, PDK4, MMP1, MMP2, MMP9, MMP13 and VEGF in ShNTC and ShANGPTL4 Spheres (ShNTC

Accepted manuscript

Spheres arbitrary set to 1, n=3). (D) 24h and 48h i*n vitro* invasion potential of ShNTC and ShANGPTL4 Spheres. (n=3). Representative photographs of the invasion potential of ShNTC and ShANPTL4 Spheres. (E) Levels of lactate, pyruvate and ATP in ShNTC and ShANGPTL4 Spheres. ATP content is expressed as relative to ShNTC (n=3) and is arbitrary set to 1. (F) Quantification of MitoTracker® and COX2 staining using Cell Health Profiling, n=3). *p<0.05, **p<0.01, ***p<0.001.

Figure 6: Involvement of ERK signaling pathway in cell invasion and PI3K signaling pathway in cell survival in HepaRG cells.

Effect of MEK1/2 inhibitor (U0126, 10µM). (A) Phase-contrast photographs, western blot of ERK and P-ERK, numbers of Spheres after seeding of 100,000 cells and LDH release for viability assessment of HepaRG-Spheres (n=3). Bar=50µm. (B) mRNA levels of OCT4, NANOG, IL-6, IL-11, PDK4, ANGPTL4, MMP1, MMP2, MMP9, MMP13, VEGF in HepaRG-Spheres treated with U0126 (untreated HepaRG-Spheres arbitrary set to 1, n=3). (C) 24h and 48h i*n vitro* invasion potential of Spheres treated with U0126. (n=3), Representative photographs of the invasion potential of HepaRG-Spheres obtained after treatment with U0126. (D) Levels of pyruvate, lactate and ATP in Spheres treated with or without U0126. ATP content is expressed as relative to untreated Spheres and is arbitrary set to 1 (n=3).*p<0.05, **p<0.01, ***p<0.001.

Effect of PI3K inhibitor (LY294002, 10µM). (E) Phase-contrast photographs, western blot of AKT, P-AKT and β-actin, numbers of HepaRG-Spheres after seeding of 100,000 cells and LDH release for viability assessment of HepaRG-Spheres (n=3). Bar=50µm. (F) mRNA levels of OCT4, NANOG, IL-6, IL-11, PDK4, ANGPTL4, MMP1, MMP2, MMP9, MMP13, VEGF in Spheres treated with LY294002 (untreated HepaRG-Spheres arbitrary set to 1, n=3). *p<0.05, **p<0.01, ***p<0.001.

Accepted manuscript

Figure 7: PDK4 inhibition combined with chemotherapy contributes to increased tumor cell death in HCC cell lines.

(A) Evaluation by the MTT assay of viability of 4-day old adherent (D4) or anchorage-independent (Spheres) HepaRG, BC2, HepG2, HuH7 cells after 3-day treatment with cisplatin (10µg/l for HepaRG, HuH7 and HepG2; 20µg/ml for BC2) or sorafenib (2.5µM for HepaRG and HuH7; 10µM for HepG2; 15µM for BC2); untreated cells arbitrary set to 100, n=3. *p<0.05, **p<0.01, ***p<0.001. (B) mRNA levels of *OCT4, NANOG, ANGPTL4, PDK4* in HepaRG-D4 (D4) and HepaRG Spheres (Spheres) treated with cisplatin or sorafenib (D4 arbitrary set to 1, n=4). *p<0.05, **p<0.01, ***p<0.001 for treated versus untreated D4 cells; ###p<0.001 for untreated Spheres versus untreated D4 and $p<0.05, $$p<0.01, $$$p<0.001 for untreated Spheres versus treated D4. (C) Viability of BC2, HepG2, HuH7, HepaRG-D4, HepaRG-D10 and HepaRG-Spheres evaluated by MTT assay after treatment with dichloroacetate (DCA, 50mM), in combination with cisplatin or sorafenib at the same concentrations as in (A) (untreated cells arbitrary set to 100, n=3). Viability of ShANGPTL4-HepaRG-Spheres treated with sorafenib (n=4). *p<0.05, **p<0.01, ***p<0.001. Viability of HepaRG-D4 transfected by siPDK4-1, siPDK4-2 or non-targeting siRNA (siNT) evaluated by MTT assay after treatment after treatment with DCA (50mM) in combination with sorafenib (2.5µM) (n=3).

Accepted manuscript

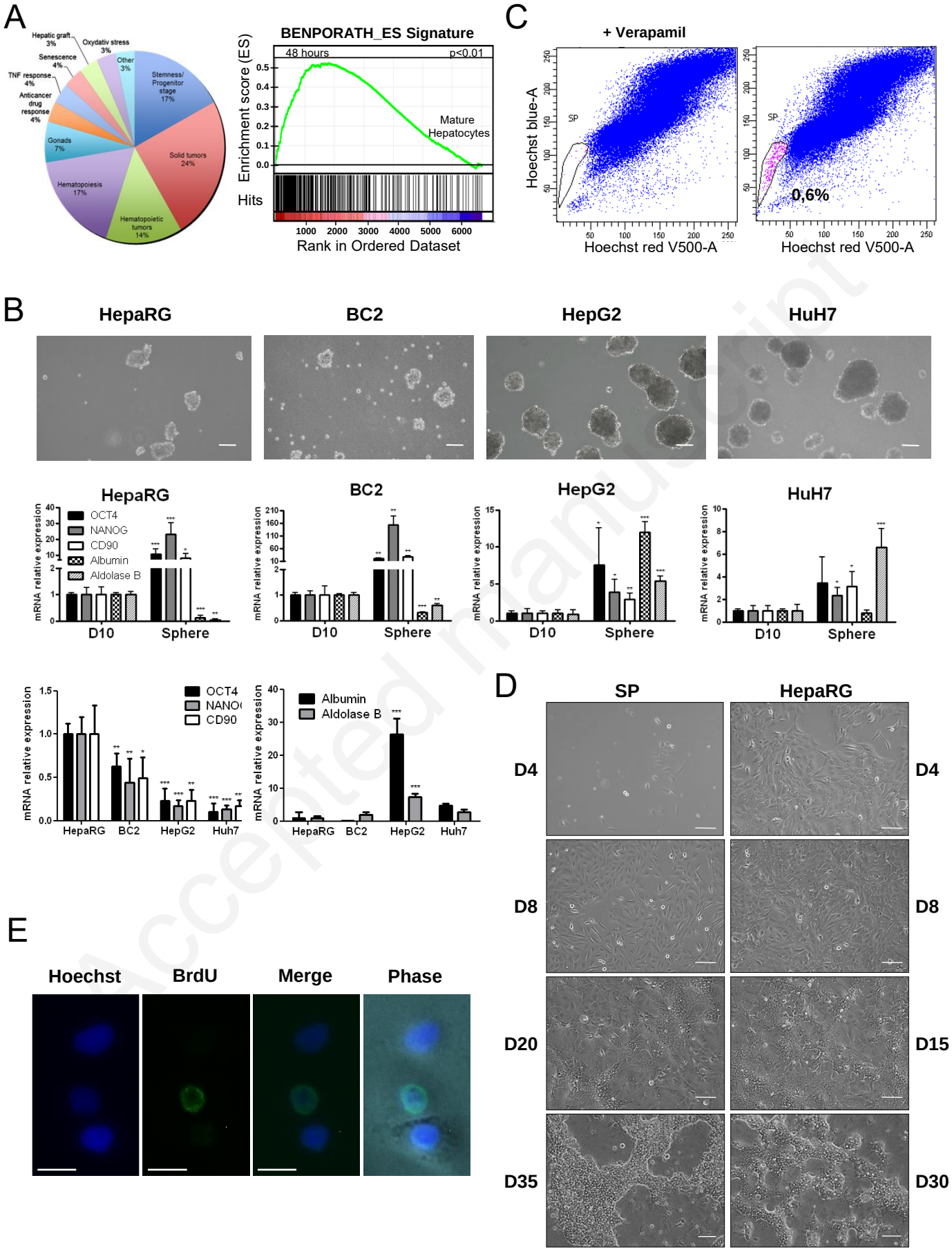

Figure 1

Accepted manuscript

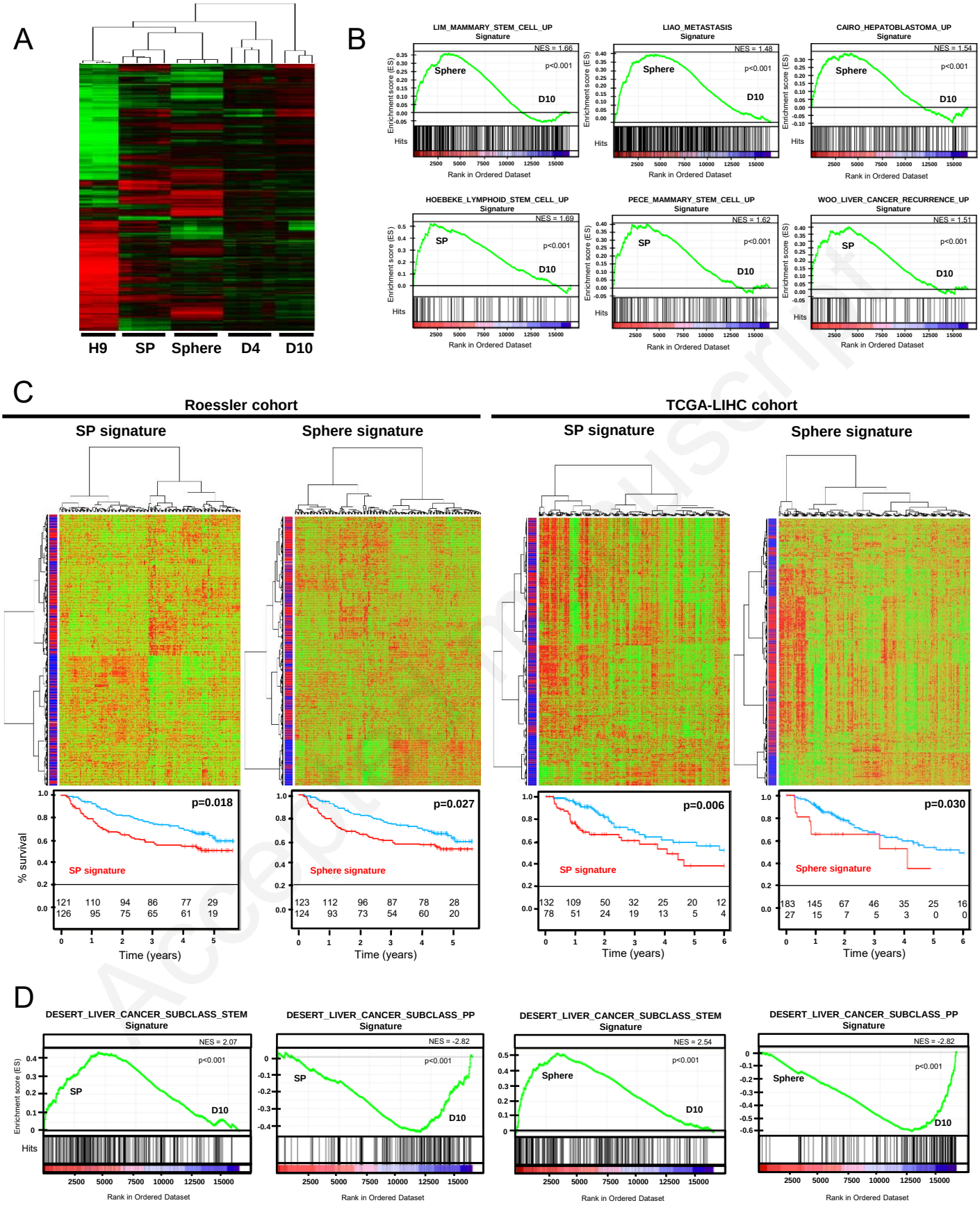
A
H9
SP
Sphere
D4
D10
B
LIM_MAMMARY_STEM_CELL_UP Signature
NES = 1.66
p<0.001
Sphere
D10
LIAO_METASTASIS Signature
NES = 1.48
p<0.001
Sphere
D10
CAIRO_HEPATOBLASTOMA_UP Signature
NES = 1.54
p<0.001
Sphere
D10
HOEBEKE_LYMPHOID_STEM_CELL_UP Signature
NES = 1.69
p<0.001
SP
D10
PECE_MAMMARY_STEM_CELL_UP Signature
NES = 1.62
p<0.001
SP
D10
WOO_LIVER_CANCER_RECURRENCE_UP Signature
NES = 1.51
p<0.001
SP
D10
Enrichment score (ES)
Hits
Rank in Ordered Dataset
C
Roessler cohort
TCGA-LIHC cohort
SP signature
Sphere signature
SP signature
Sphere signature
% survival
p=0.018
SP signature
121 110 94 86 77 29
126 95 75 65 61 19
p=0.027
Sphere signature
123 112 96 87 78 28
124 93 73 54 60 20
p=0.006
SP signature
132 109 50 32 25 20 12
78 51 24 19 13 5 4
p=0.030
Sphere signature
183 145 67 46 35 25 16
27 15 7 5 3 0 0
Time (years)
D
DESERT_LIVER_CANCER_SUBCLASS_STEM Signature
NES = 2.07
p<0.001
SP
D10
DESERT_LIVER_CANCER_SUBCLASS_PP Signature
NES = -2.82
p<0.001
SP
D10
DESERT_LIVER_CANCER_SUBCLASS_STEM Signature
NES = 2.54
p<0.001
Sphere
D10
DESERT_LIVER_CANCER_SUBCLASS_PP Signature
NES = -2.82
p<0.001
Sphere
D10
Enrichment score (ES)
Hits
Rank in Ordered Dataset

Figure 2

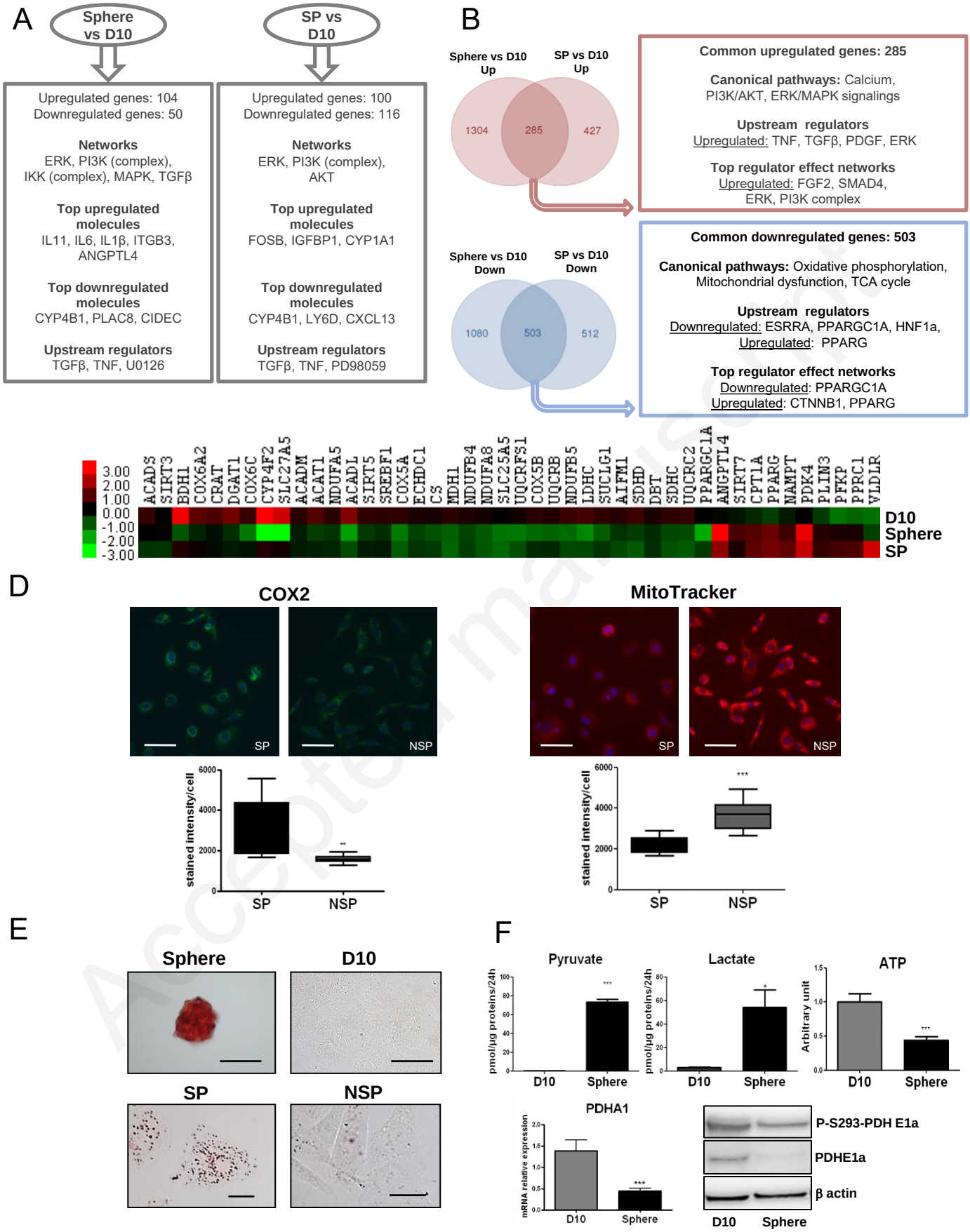
A
Sphere vs D10
SP vs D10
Upregulated genes: 104
Downregulated genes: 50
Networks
ERK, PI3K (complex), IKK (complex), MAPK, TGFβ
Top upregulated molecules
IL11, IL6, IL1β, ITGB3, ANGPTL4
Top downregulated molecules
CYP4B1, PLAC8, CIDEC
Upstream regulators
TGFβ, TNF, U0126
Upregulated genes: 100
Downregulated genes: 116
Networks
ERK, PI3K (complex), AKT
Top upregulated molecules
FOSB, IGFBP1, CYP1A1
Top downregulated molecules
CYP4B1, LY6D, CXCL13
Upstream regulators
TGFβ, TNF, PD98059
B
Sphere vs D10 Up
SP vs D10 Up
1304
285
427
Common upregulated genes: 285
Canonical pathways: Calcium, PI3K/AKT, ERK/MAPK signalings
Upstream regulators
Upregulated: TNF, TGFβ, PDGF, ERK
Top regulator effect networks
Upregulated: FGF2, SMAD4, ERK, PI3K complex
Sphere vs D10 Down
SP vs D10 Down
1080
503
512
Common downregulated genes: 503
Canonical pathways: Oxidative phosphorylation, Mitochondrial dysfunction, TCA cycle
Upstream regulators
Downregulated: ESRRA, PPARGC1A, HNF1a,
Upregulated: PPARG
Top regulator effect networks
Downregulated: PPARGC1A
Upregulated: CTNNB1, PPARG
3.00
2.00
1.00
0.00
-1.00
-2.00
-3.00
ACADS SIRT3 BDH1 COX6A2 CRAT DGAT1 COX6C CYP4F2 SLC27A5 ACADM ACAT1 MDUFA5 ACADL SIRT5 SREBF1 COX5A ECHDC1 CS MDH1 MDUFB4 MDUFA8 SLC25A5 UQCRFS1 COX5B UQCRB MDUFB5 LDHC SUCLG1 AIFM1 SDHD DBT SDHC UQCRC2 PPARGC1A ANGPTL4 SIRT7 CPT1A PPARG NAMPT PDK4 PLIN3 PFKP PPRC1 VLDLR
D10
Sphere
SP
D
COX2
MitoTracker
SP
NSP
SP
NSP
stained intensity/cell
6000
4000
2000
0
**
***
SP
NSP
E
Sphere
D10
SP
NSP
F
Pyruvate
Lactate
ATP
pmol/µg proteins/24h
Arbitrary unit
D10
Sphere
PDHA1
mRNA relative expression
P-S293-PDH E1a
PDHE1a
β actin

Figure 3

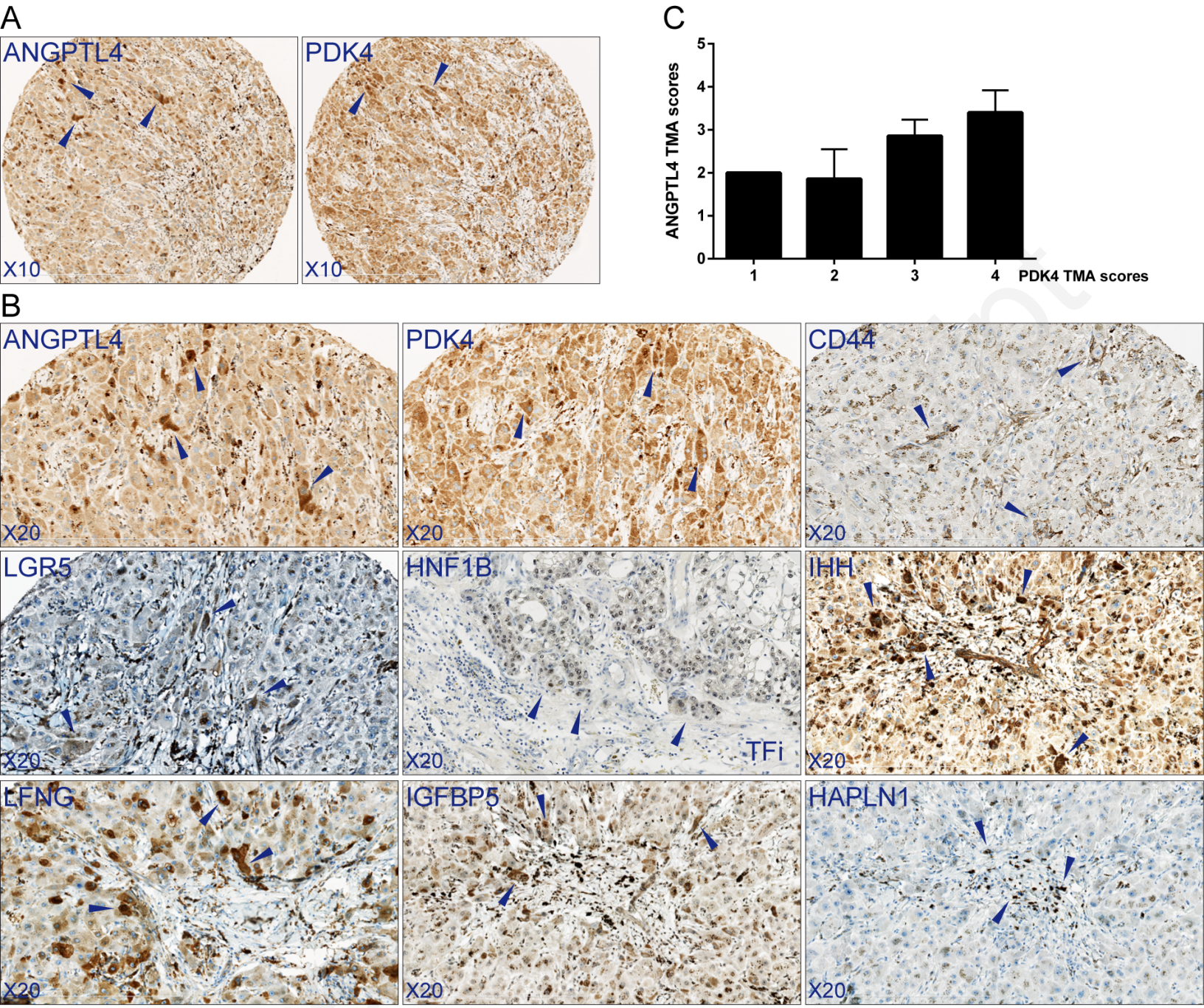
A
ANGPTL4
X10
PDK4
X10
C
ANGPTL4 TMA scores
0
1
2
3
4
5
1
2
3
4
PDK4 TMA scores
B
ANGPTL4
X20
PDK4
X20
CD44
X20
LGR5
X20
HNF1B
X20
TFi
IHH
X20
LFNG
X20
IGFBP5
X20
HAPLN1
X20
D
LGR5
IHH
CD44
PDK4
ANGPTL4
IGBP5
LFNG
HNF1B
HAPLN1
E
ANGPTL4
P = 0.03
Relative TMA scores
No T necrosis
T necrosis
PDK4
P = 0.01
Relative TMA scores
No T necrosis
T necrosis

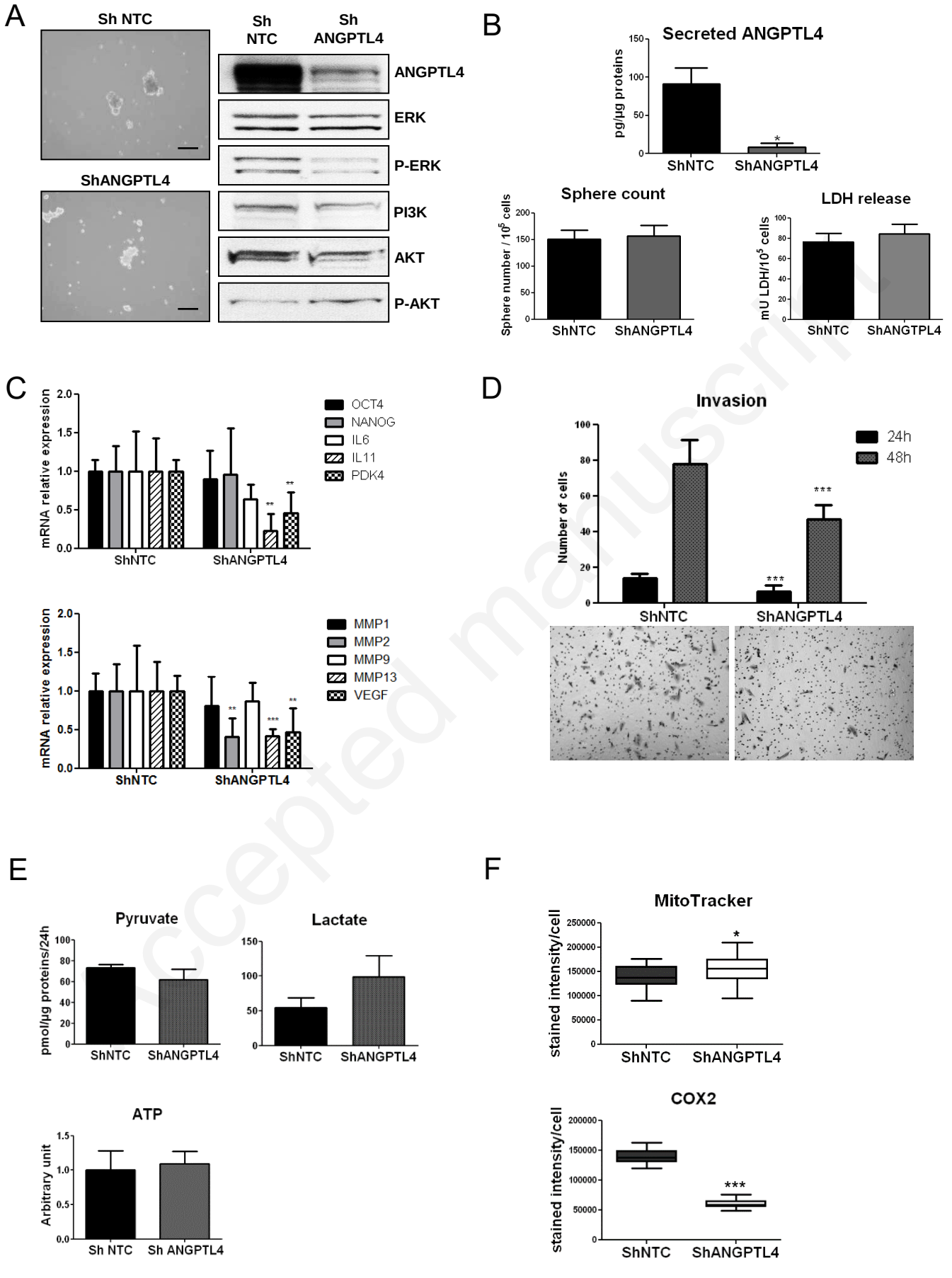

Figure 5

Accepted manuscript

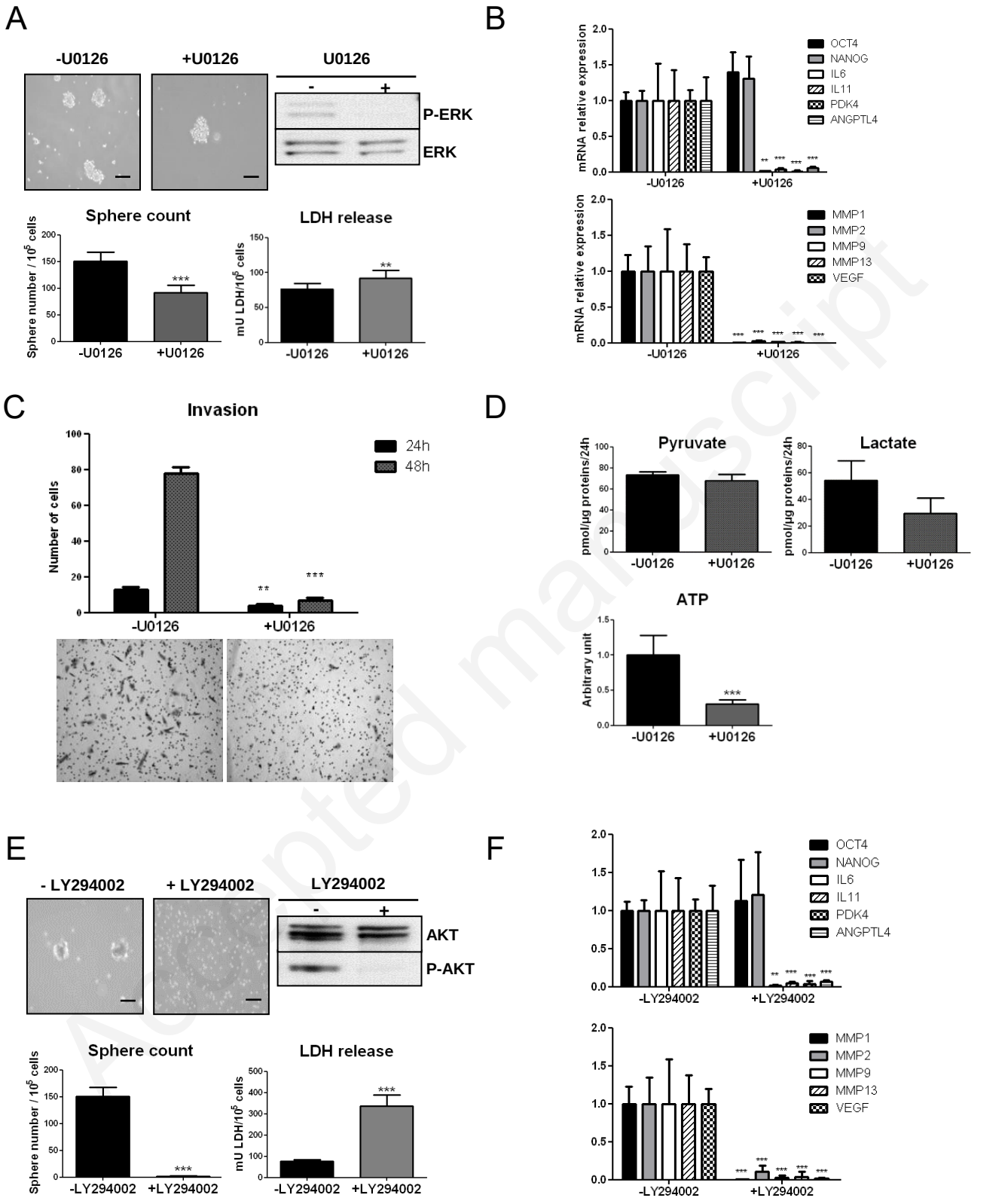

Accepted manuscript

Figure 6

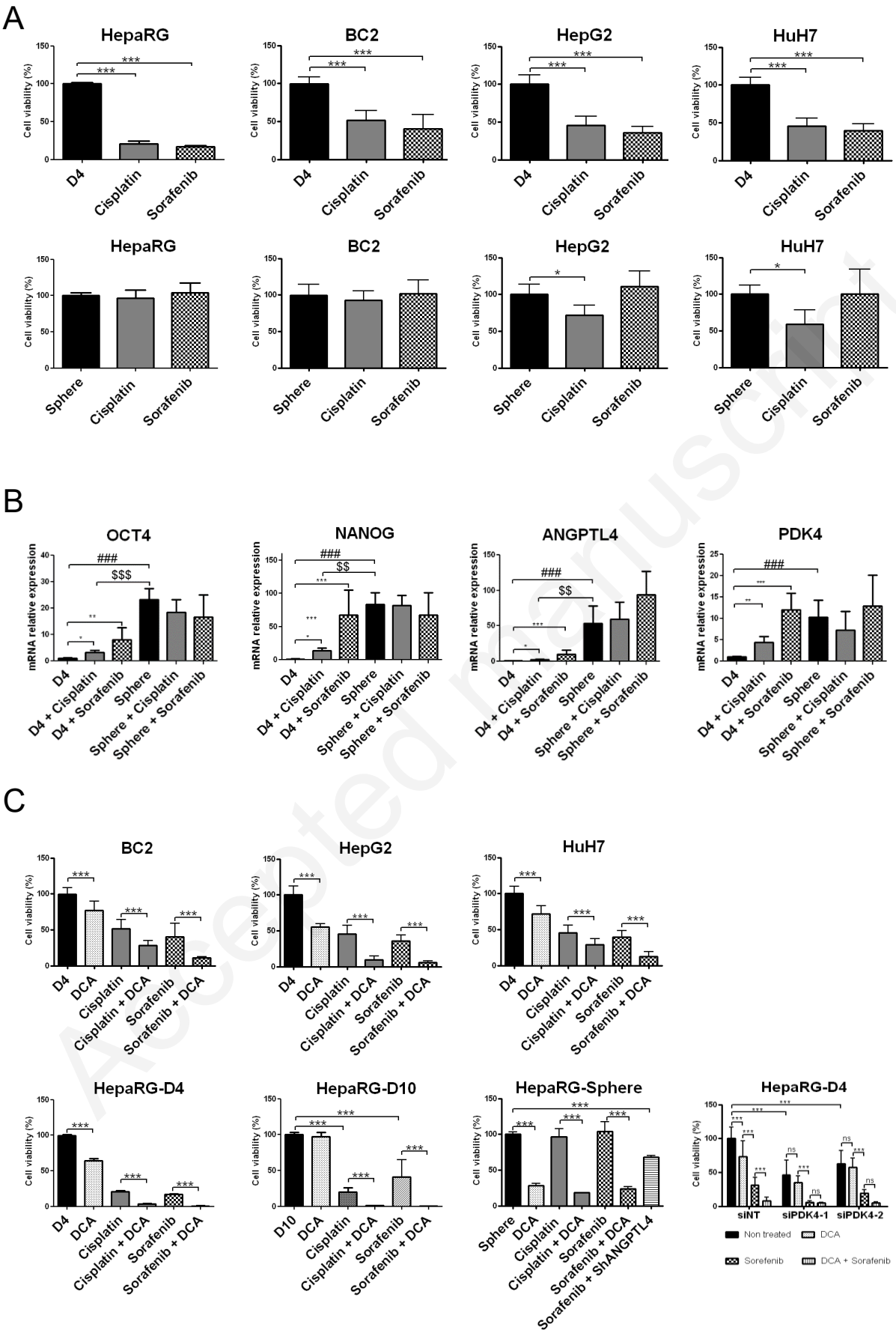

Figure 7

Accepted manuscript

Downloaded from cancerres.aacrjournals.org on March 5, 2019. © 2019 American Association for Cancer Research.